

## Single-proton and core-coupled states in $^{133}\text{Sb}$

M. Sanchez-Vega,<sup>1</sup> B. Fogelberg,<sup>1</sup> H. Mach,<sup>1</sup> R. B. E. Taylor,<sup>1,\*</sup> A. Lindroth,<sup>1</sup> J. Blomqvist,<sup>2</sup> A. Covello,<sup>3</sup>  
and A. Gargano<sup>3</sup>

<sup>1</sup>*Department of Neutron Research, Uppsala University, S-61182 Nyköping, Sweden*

<sup>2</sup>*Department of Physics Frescati, Royal Institute of Technology, Frescativägen 24, S-10405 Stockholm, Sweden*

<sup>3</sup>*Dipartimento di Scienze Fisiche, Università di Napoli Federico II, Complesso Universitario di Monte S. Angelo,  
Via Cintia, I-80126 Napoli, Italy*

*and Istituto Nazionale di Fisica Nucleare, Complesso Universitario di Monte S. Angelo, Via Cintia, I-80126 Napoli, Italy*

(Received 23 December 1998; published 30 June 1999)

The low-energy structure of the  $Z=51$ ,  $N=82$  nuclide  $^{133}\text{Sb}$  has been studied through a high-sensitivity investigation of the  $\beta^-$  decay of  $^{133}\text{Sn}$ . As a result, more than 70 new excited states have been observed and about 100  $\gamma$ -ray transitions have been placed in the level scheme. Regarding the single-proton states, the  $d_{3/2}$  level was found at 2439.5 keV and for the  $h_{11/2}$  state at 2791.3 keV, a half-life of 11.4(4.5) ps has been measured. Levels at higher energies are interpreted as core-coupled states with the  $g_{7/2}$  odd proton coupled to the excited states of the  $^{132}\text{Sn}$  core. A detailed discussion of the beta decay is presented.

[S0556-2813(99)05107-9]

PACS number(s): 21.10.-k, 23.20.Lv, 21.60.Cs, 27.60.+j

### I. INTRODUCTION

The nuclei consisting of one valence particle outside a doubly closed shell (DCS) core have played an essential role in testing the nuclear shell model predictions. The particularly simple structure of these nuclei is reflected in their observed low-energy spectra which is interpreted as consisting of two types of states: excitations of a single particle and states made up from the coupling of the valence nucleon to excitations of the core.

Despite the importance of these nuclides in the description of nuclear structure, the available experimental information is rather scarce. The largest amount of data exists at the DCS regions with  $A < 56$  and at  $^{208}\text{Pb}$ . Additional data in-between these regions must be sought far away from the valley of  $\beta$  stability in the vicinity of the DCS nuclei  $^{78}\text{Ni}$ ,  $^{100}\text{Sn}$ , and  $^{132}\text{Sn}$ . Although these new regions are studied within the same theoretical framework, presently only at  $^{132}\text{Sn}$ , it is possible to investigate experimentally the low energy structure of the single-particle nuclei. Spectroscopic studies of  $\beta$ -decays at on-line fission product mass-separators have proved to be the most efficient tool to obtain new experimental data on the neutron-rich nuclei close to  $^{132}\text{Sn}$ . Recent examples of this type of work include the identification [1] of single neutron states in  $^{133}\text{Sn}$ , the determination [2] of effective charges in the region, and a measurement [3] of the  $g_{7/2}$  single-proton magnetic moment. Studies of prompt  $\gamma$ -rays emitted in spontaneous fission [4–6] using large  $\gamma$ -ray detector arrays, are also providing new information on the  $^{132}\text{Sn}$  region.

We have taken advantage of the developments of the target-ion source system at the on-line mass separator at

Studsvik to conduct a considerably more sensitive investigation of the  $\beta^-$ -decay of  $^{133}\text{Sn}$  than in previous works [7,9]. In the present experiment more than 70 new excited states and about 100  $\gamma$ -ray transitions have been identified in the single-proton  $^{133}\text{Sb}$  nucleus. Consequently the level scheme has been extended considerably. New results on single-proton levels and transition rates in  $^{133}\text{Sb}$  (in comparison to their counterparts in the  $^{208}\text{Pb}$  region) have already been discussed in Ref. [10]. In the present paper, we provide a full account of the results.

### II. EXPERIMENTAL TECHNIQUES

#### A. Multispectrum scaling (MSS)

The Sn isotopes were produced by thermal neutron induced fission of  $^{235}\text{U}$  at the OSIRIS-ISOL on line mass-separator [11] at Studsvik in Sweden. After mass separation the  $A=133$  beam was deposited onto an Al-coated Mylar tape which was periodically moved to minimize the collection of long-lived isobars. Nevertheless, the  $\gamma$ -ray transitions belonging to the  $^{133}\text{Sb} \rightarrow ^{133}\text{Te}$  decay ( $T_{1/2} = 2.5$  min) appear in our singles spectra with significant intensities compared to the transitions of interest following the  $^{133}\text{Sn} \rightarrow ^{133}\text{Sb}$  decay ( $T_{1/2} = 1.4$  s). In order to identify the latter transitions, a multi spectrum scaling (MSS) experiment was performed, using a Compton suppressed 50% Ge detector. It consisted of a series of consecutive  $\gamma$ -ray singles spectra that were recorded as a function of time following beam collection. In this way more than 100  $\gamma$ -ray transitions were identified in  $^{133}\text{Sb}$ . An accurate determination of  $\gamma$ -ray energies and intensities (see Table I) was obtained through an energy calibration which included at lower energies the well known [12]  $\gamma$ -rays belonging to the daughter  $^{133}\text{Te}$  activity, and at higher energies via the 6–7 MeV Fe neutron capture  $\gamma$  lines [13] that were part of the background radiation. The  $^{152}\text{Eu}$  and absolutely calibrated  $^{60}\text{Co}$  sources were used to obtain the efficiency calibration at low energies, while the 6.129

\*Present address: Nuclear Physics Group, Schuster Laboratory, University of Manchester, Brunswick Street, Manchester, M13 9PL, U.K.

TABLE I. Data for  $\gamma$ -rays observed in the  $\beta$ -decay of  $^{133}\text{Sn}$ . The  $\gamma$ -rays having relative intensities  $\geq 0.4$  units, which exceed the sensitivity limit of the coincidence measurement, are presumed to be ground state transitions (labeled by “g”) if no coincidence relation was observed. The transitions with  $E_\gamma > 6$  MeV are all assumed to feed the ground state, since alternative placements would imply an unphysical  $\beta$ -strength.

Energy (keV)	Relative <sup>a</sup> intensity	Coincident transitions <sup>b</sup> (keV)	Initial level (keV)	Energy (keV)	Relative <sup>a</sup> intensity	Coincident transitions <sup>b</sup> (keV)	Initial level (keV)
855.6(2)	3.6(3)	1503, 2791	5149.4	4324.9(5)	0.35(7)		
962.1(2)	1000(50)	1477, 1503, 1830, 2685 3222, 3575, 3688, 3838 3868, 3940, 4039, 4078 4156, 4162, 4229, 4314 4523, 4531, 4598, 4651 4683, 4886	962.1	4522.8(2)	3.0(2)	962	5485.0
				4531.0(7)	0.40(8)	962	5493.5
				4572.7(2)	1.3(2)	g	4572.7
				4597.8(2)	10.6(7)	962	5559.9
				4634.6(7)	0.5(2)	g	4634.6
				4650.9(5)	0.30(8)	962	5612.2
1318.1(2)	1.1(1)	1503, 2791	5612.2	4683.1(3)	0.49(9)	962	5645.4
1477.1(2)	7.9(5)	962, 2685, 3205	2439.4	4701.2(4)	0.36(9)		
1502.6(2)	4.5(3)	856, 1318, 2791	4293.9	4785.9(3)	1.1(1)	g	4785.9
1829.6(15)	0.3(1)	962	2791.3	4802.1(2)	6.5(5)	g	4802.1
2106.7(3)	1.1(1)	2791	4898.0	4873.3(11)	0.18(8)		
2358.3(2)	4.6(3)	2791	5149.4	4886.4(5)	0.44(8)	962	5848.6
2376.0(2)	1.2(1)	2791	5167.4	4902.2(2)	4.2(3)	g	4902.2
2439.5(2)	8.9(6)	2685, 3205	2439.4	4937.2(3)	1.0(1)	g	4937.2
2685.0(2)	1.4(2)	962, 1477, 2440	5124.6	5001.5(2)	1.7(2)	g	5001.5
2791.3(2)	19(1)	856, 1318, 1503, 2107 2359, 2375, 2820, 3090 3275, 3282, 3980	2791.3	5039.7(2)	1.5(2)	g	5039.7
				5119.3(3)	1.7(2)	g	5118.8
				5124.7(2)	3.6(3)	g	5124.6
2821.1(2)	3.6(3)	2791	5612.2	5149.4(2)	35(2)	g	5149.4
3061.2(5)	0.22(8)			5167.4(2)	1.4(1)	g	5167.4
3073.8(13)	0.23(9)			5191.4(9)	0.20(6)	g	5191.1
3089.8(3)	0.7(1)	2791	5881.4	5276.6(2)	5.7(4)	g	5276.6
3205.4(3)	0.8(1)	1477, 2440	5645.4	5302.6(2)	1.8(2)	g	5302.6
3222.0(5)	0.32(7)	962	4183.9	5325.6(5)	0.38(8)		
3275.7(2)	3.1(3)	2791	6067.5	5376.0(2)	8.8(6)	g	5376.0
3282.3(3)	0.66(9)	962	4244.5	5402.5(7)	0.4(1)		
3574.7(2)	1.6(2)	962	4536.9	5413.2(4)	1.1(1)	g	5413.2
3687.8(3)	0.55(9)	962	4650.1	5421.4(15)	0.4(1)	g	5421.4
3822.6(3)	0.53(8)		3822.6 <sup>c</sup>	5427.8(15)	0.2(1)		
3838.4(2)	1.0(1)	962	4802.1	5450.9(8)	0.15(8)		
3867.8(4)	0.30(9)	962	4830.0	5483.1(2)	10.2(7)	g	5483.1
3940.1(2)	1.2(2)	962	4902.2	5493.8(7)	0.5(1)	g	5493.5
3979.3(5)	0.27(6)	2791	6770.6	5548.3(4)	0.37(9)		
4028.7(2)	1.5(2)	g	4028.7	5559.8(2)	8.7(6)	g	5559.9
4039.4(5)	0.37(8)	962	5001.5	5593.2(4)	0.4(1)	g	5593.2
4060.2(4)	0.37(8)			5603.3(2)	4.9(4)	g	5603.3
4077.7(5)	0.33(7)	962	5039.7	5612.2(2)	26(2)	g	5612.2
4156.1(2)	1.8(2)	962	5118.8	5645.3(2)	9.8(6)	g	5645.4
4162.2(2)	6.3(5)	962	5124.6	5684.1(3)	1.4(1)	g	5684.1
4183.7(3)	0.9(1)	g	4183.9	5692.5(5)	0.39(7)		
4209.9(5)	0.4(1)		4209.9	5742.4(3)	1.3(1)	g	5742.4
4215.2(2)	3.1(3)	g	4215.2	5750.0(5)	0.43(7)	g	5750.0
4228.5(3)	0.64(9)	962	5191.1	5790.1(2)	1.3(1)	g	5790.1
4258.0(7)	0.20(6)			5835.1(6)	0.5(1)	g	5835.1
4290.0(3)	0.5(1)	g	4290.0	5841.1(6)	0.4(1)	g	5841.1
4296.1(2)	1.8(2)	g	4296.1	5881.4(2)	3.3(3)	g	5881.4
4307.3(2)	2.2(2)	g	4307.3	5920.8(5)	0.43(8)	g	5920.8
4314.4(2)	1.9(2)	962	5276.6	5928.5(3)	1.1(1)	g	5928.5

TABLE I. (*Continued.*)

Energy (keV)	Relative <sup>a</sup> intensity	Coincident transitions <sup>b</sup> (keV)	Initial level (keV)	Energy (keV)	Relative <sup>a</sup> intensity	Coincident transitions <sup>b</sup> (keV)	Initial level (keV)
5938.2(3)	1.0(1)	g	5938.2	6264.3(5)	0.29(5)	g	6264.3
5960.1(2)	1.8(2)	g	5960.1	6286.3(11)	0.11(4)	g	6286.3
5970.8(2)	3.9(3)	g	5970.8	6314.8(2)	5.9(4)	g	6314.8
5977.6(6)	0.5(1)	g	5977.6	6326.6(4)	0.41(6)	g	6326.6
6059.4(3)	1.7(2)	g	6059.4	6348.8(2)	2.2(2)	g	6348.8
6068.0(3)	1.5(1)	g	6067.5	6364.2(3)	0.73(8)	g	6364.2
6074.8(8)	0.41(8)	g	6074.8	6411.5(3)	0.83(9)	g	6411.5
6093.3(2)	6.7(5)	g	6093.3	6445.1(3)	0.81(9)	g	6445.1
6102.5(3)	2.1(2)	g	6102.5	6457.7(2)	1.4(1)	g	6457.7
6112.4(2)	7.9(5)	g	6112.4	6497.9(3)	0.68(9)	g	6497.9
6124.0(2)	4.7(3)	g	6124.0	6505.4(3)	0.9(1)	g	6505.4
6136.1(7)	0.24(6)	g	6136.1	6514.9(3)	0.56(7)	g	6514.9
6170.1(2)	2.7(2)	g	6170.1	6576.2(6)	0.23(4)	g	6576.2
6200.3(4)	0.51(7)	g	6200.3	6705.7(6)	0.15(5)	g	6705.7
6238.9(14)	0.09(4)	g	6238.9	6794.4(6)	0.16(4)	g	6794.4
6251.9(4)	0.36(6)	g	6251.9	6950.7(5)	0.32(6)	g	6950.7

<sup>a</sup>To get  $I_\gamma$  in % per decay of parent nucleus multiply by 0.012(2) [9].

<sup>b</sup>Coincident  $\gamma$ -rays are listed for all transitions selected as gates.

<sup>c</sup>This transition was not seen in coincidence with other lines; it may possibly define a level at this energy.

MeV  $\gamma$ -ray [14] emitted in the  $^{13}\text{C}(\alpha, n)^{16}\text{O}$  reaction at a known rate, provided the calibration at high energies. The MSS analysis allowed the identification of  $\gamma$ -rays having intensities down to about  $10^{-5}$  per decay of the  $^{133}\text{Sn}$  parent nucleus.

### B. $\gamma\gamma$ coincidences

A similar experimental sensitivity as in the MSS experiment was required in the  $\gamma\gamma$  coincidence measurements to build the level scheme of  $^{133}\text{Sb}$ . It is known from previous works [7–9] that the high lying states of  $^{133}\text{Sb}$  are very weakly populated in the  $\beta^-$ -decay of  $^{133}\text{Sn}$ . Due to experimental constraints the  $\gamma\gamma$  coincidence data have been collected in three separate runs (run I, II, and III) using either two or three Ge detectors in the setup. Each detector was shielded with 5 mm Al to absorb  $\beta$  particles. In the first run, three Ge detectors of efficiencies 17%, 20%, and 80% were positioned in a plane around the collection point. Radioactive sources were collected on a tape, which was used to remove old samples at time intervals of 2.5 s. In run II a large volume (80%) Ge detector and a 50% Ge spectrometer with BGO anti-Compton shielding were placed in the same axis, at distances of 10 and 12 cm, respectively, away from the source. The tape cycle time in this case was set to 5 s. The largest amount of coincidence data was obtained in run III ( $>6.3 \times 10^7$  coincidences in addition to  $\sim 3.3 \times 10^7$  events from run I and only  $3.3 \times 10^6$  events from run II). In this case the 17% Ge detector of run I was replaced by the Compton suppressed 50% Ge spectrometer. The tape cycle time for run III was 2.4 s. The analysis consisted of sorting the coincidence gates for all detector combinations and for every run

separately. The resulting coincidence spectra obtained from gating on a given  $\gamma$ -ray transition, were gain-shifted and added in order to increase the statistical accuracy (see Fig. 1). A presentation of  $\gamma$ -ray transition energies, intensities and coincidence relations observed in  $^{133}\text{Sb}$  is given in Table I. The lowest  $\gamma$ -ray intensity seen in our coincidence data is of the order of  $2-4 \times 10^{-5}$  per decay of the parent  $^{133}\text{Sn}$ .

### C. Fast timing $\beta\gamma\gamma(t)$

The sensitive fast-timing  $\beta\gamma\gamma(t)$  method described in [15] was used to measure the half-life of the single-proton  $h_{11/2}$  level at 2791.3 keV. The experimental setup consisted

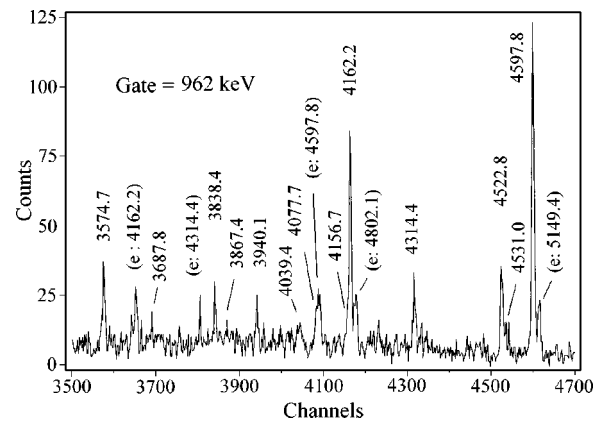


FIG. 1. Section of the  $\gamma\gamma$ -coincidence spectrum obtained by gating on the 962-keV  $\gamma$ -ray transition. The single and double escape peaks due to higher energy  $\gamma$  transitions are given in parentheses.

of a 3 mm NE111A plastic scintillator for detecting  $\beta$  particles, a small BaF<sub>2</sub> crystal and a high resolution (80%) Ge detector for  $\gamma$ -rays. All detectors were placed around the beam deposition point in a rather close geometry. The time delay between events observed in the two fast timing  $\beta$  and BaF<sub>2</sub> scintillators provided the timing information while coincidence with a  $\gamma$ -ray in the Ge detector allowed for a selection of the decay path. The coincidence spectrum gated on the 2791.3 keV transition revealed that the  $h_{11/2}$  level is populated by four main  $\gamma$ -rays of energies 1502.6, 2358.3, 2821.1, and 3275.7 keV, respectively, from higher lying levels. This  $\gamma$ -ray population of the  $h_{11/2}$  single-proton state allowed to measure the level half-life using the centroid shift technique [15]. The measurement followed a classical scheme of two sequential  $\gamma$ -ray transitions. When the  $\gamma$ -ray deexciting the level,  $\gamma_{2791}$ , is gated in the Ge detector and the feeding  $\gamma$ -ray,  $\gamma_{\text{feed}}$ , is gated in the BaF<sub>2</sub> crystal, the centroid shift of the fast timing  $\beta$ - $\gamma_{\text{feed}}$  spectrum provides a reference point:  $t_{\text{ref}} = \tau'_0 + \tau_{\text{feed}}$ . If one inverts the gates and selects  $\gamma_{\text{feed}}$  in the Ge detector and  $\gamma_{2791}$  in BaF<sub>2</sub>, then the fast timing  $\beta$ - $\gamma_{2791}$  spectrum is time-delayed by a shift equal to  $t = \tau''_0 + \tau_{\text{feed}} + \tau_{2791}$ . The points  $\tau'_0$  and  $\tau''_0$  represent a fixed time delay between timing detectors, which is energy dependent. Since the average energy of the transitions feeding the  $h_{11/2}$  level is exceptionally close to the energy of 2791.3 keV for the deexciting transition,  $\tau'_0$  is equal to  $\tau''_0$  and no further corrections are required in the analysis. Thus the mean life of the 2791.3 keV level is precisely equal to the shift between the time-delayed and reference points, since any influence from the mean life of the higher lying level,  $\tau_{\text{feed}}$ , is canceled in the comparison.

In order to improve the statistical accuracy, gates on the full energy peak and part of its Compton continuum in the energy range above 1 MeV were selected in the BaF<sub>2</sub> detector. The  $\gamma\gamma$ -coincidence data have certified that there are no impurity contributions in the selected range. As a consistency check, and to improve the statistical accuracy, the parallel  $\gamma$ -transitions feeding the  $d_{5/2}$  level at 962.1 keV were also used to provide independently the time reference points, see also Ref. [10]. As a result the half-life of the single-proton  $h_{11/2}$  state was measured as  $T_{1/2} = 11.4(4.5)$  ps.

Since the electronics was optimized for measuring the lifetime of the  $h_{11/2}$  state at 2791.3 keV and was set to accept energy signals of  $E > 1$  MeV, no half life result was obtained for the  $d_{5/2}$  level at 962.1 keV.

### III. RESULTS AND DISCUSSION

The energy spectrum of the  $Z=51$ ,  $N=82$   $^{133}\text{Sb}$  nucleus is somewhat different from single-particle spectra at other DCS regions, since the single-proton levels that appear at the lowest energies, are separated by a rather wide energy gap from other more complicated type of states. This is due to the stiffness of the  $^{132}\text{Sn}$  core where the first excited state  $2^+$  lies at 4041.1 keV. Therefore the lowest core-coupled states in  $^{133}\text{Sb}$  are expected to appear at approximately 4 MeV while the highest single-proton level, either the  $h_{11/2}$  at 2791.3 keV or the still unknown  $s_{1/2}$  state, is predicted at

TABLE II. Experimental single-proton energies in  $^{133}\text{Sb}$  (in MeV) compared with theoretical calculations: WS+ $\Delta$  from Ref. [17], WS, FY, and SIII from [18], SKX Ref. [19], and RSM.

Orbitals	Expt.	Theoretical values					
		WS+ $\Delta$	WS	FY	SIII	SKX	RSM
$h_{11/2}$	2.79	2.87	2.16	2.23	3.54	2.83	2.96
$d_{3/2}$	2.44	2.05	2.57	3.21	3.80	2.42	2.37
$s_{1/2}$		1.90	2.84	3.14	4.62	2.95	2.47
$d_{5/2}$	0.96	0.36	0.05	0.44	1.67	0.56	0.78
$g_{7/2}$	0.00	0.00	0.00	0.00	0.00	0.00	0.00

2–3 MeV (see discussion in the next subsection). Due to this separation the single-proton states in  $^{133}\text{Sb}$  are expected to have rather pure single-particle configurations. Both single-proton and core-coupled states are populated in the  $\beta^-$ -decay of  $^{133}\text{Sn}$  and will be discussed separately below, while the deduced strength of  $\beta$  transitions in the decay of  $^{133}\text{Sn}$  is considered in Sec. III C.

#### A. Single-proton states

The available single-proton states in the  $50 < Z < 82$  shell correspond to the  $g_{7/2}$ ,  $d_{5/2}$ ,  $d_{3/2}$ ,  $s_{1/2}$ , and  $h_{11/2}$  orbitals. From the early work of Ref. [7] and the data [12] on the  $\beta^-$ -decay to  $^{133}\text{Te}$ , the single proton  $g_{7/2}$  configuration is assigned to the ground state of  $^{133}\text{Sb}$ . The  $d_{5/2}$  and  $h_{11/2}$  single proton states were previously established [7,8] at 962.1 keV and 2791.3 keV, respectively. In the present experiment a new single-proton state was found at 2439.5 keV, decaying to the  $d_{5/2}$  level at 962.1 keV and to the  $g_{7/2}$  ground state. The decay pattern suggests that this new level is indeed the  $d_{3/2}$  single-proton state and not the  $s_{1/2}$ , which therefore remains unobserved. A previous experimental study [9] reported a 2707.7 keV  $\gamma$ -ray, which was tentatively assigned as the ground state transition from the  $d_{3/2}$  level. No 2707.7 keV  $\gamma$ -ray was observed in the present study despite about two orders of magnitude higher sensitivity than in Ref. [9]. The previously observed 2707.7 keV line most likely did not belong to  $^{133}\text{Sb}$ .

We could not identify any  $\gamma$ -ray that would indicate the decay of the expected  $s_{1/2}$  single-proton level. From our data we estimate a population of this state in the  $\beta^-$  decay of  $^{133}\text{Sn}$  to be at least a factor of 20 smaller than the  $d_{3/2}$  level. This is reasonable considering the high angular momentum,  $7/2^-$ , of the parent  $^{133}\text{Sn}$  nucleus. An alternative method to populate the  $s_{1/2}$  state is via the  $\beta^-$  delayed-neutron emission of  $^{134}\text{Sn}$ . This method has already been applied [1] to the study of single neutron states in  $^{133}\text{Sn}$ . The  $\beta^-$ -decay of  $^{134}\text{In}$  is characterized by a wide energy window and a high probability for delayed neutron emission,  $P_n$ , which allows [1] the feeding of the low-energy states in  $^{133}\text{Sn}$ . The energy window for delayed neutron emission in the  $\beta^-$ -decay of  $^{134}\text{Sn}$  is about 4 MeV [16], making it possible to populate the low-energy levels in  $^{133}\text{Sb}$ , including the “missing”  $s_{1/2}$  state. Inspection of data recently obtained for the  $A=134$  isobars [2] shows a substantial neutron population of the  $d_{5/2}$

TABLE III. Beta transition strengths in the  $^{133}\text{Sn}$  decay.

$J^\pi$	$E_{\text{level}}$ (keV)	$\log f_0 t^a$	$1/f_0 t(10^{-6})$	$J^\pi$	$E_{\text{level}}$ (keV)	$\log f_0 t^a$	$1/f_0 t(10^{-6})$
$7/2^+$	0.0	5.44	3.66		5593.2	7.40	0.04
$5/2^+$	962.1	6.05	0.90		5603.3	6.33	0.46
$3/2^+$ <sup>b</sup>	2439.5	7.42	0.04	$(9/2^-)$	5612.2	5.53	2.96
$11/2^-$	2791.3	>8.53	<0.003	$(5/2)$	5645.4	5.89	1.28
	4028.7	7.77	0.02		5684.1	6.81	0.15
	4060.2	8.38	0.004		5692.5	7.32	0.05
	4183.9	7.79	0.02		5742.4	6.76	0.17
	4209.9	8.24	0.006		5750.0	7.24	0.06
	4215.2	7.37	0.04		5790.1	6.73	0.19
	4244.5	7.99	0.008		5835.1	7.16	0.07
	4258.0	8.59	0.003		5841.1	7.16	0.07
	4290.0	8.11	0.008		5848.6	7.16	0.07
$(11/2, 13/2)$	4293.9	>8.59	<0.003	$(9/2)$	5881.4	6.18	0.67
	4296.1	7.54	0.03		5920.8	7.16	0.07
	4307.3	7.47	0.03		5928.5	6.74	0.18
	4324.9	8.28	0.005		5938.2	6.78	0.17
	4536.9	7.51	0.03		5960.1	6.43	0.37
	4572.7	7.52	0.03		5970.8	6.10	0.79
	4634.6	7.95	0.01		5977.6	7.00	0.10
	4650.1	6.86	0.14		6059.4	6.39	0.41
	4701.2	8.07	0.008	$(9/2)$	6067.5	5.95	1.13
	4785.9	7.47	0.03		6074.8	6.99	0.10
	4802.1	6.66	0.22		6093.3	5.78	1.67
	4830.0	8.01	0.01		6102.5	6.29	0.51
	4873.3	8.26	0.006		6112.4	5.71	1.93
$(9/2, 11/2)$	4898.0	7.44	0.04		6124.0	5.93	1.17
	4902.2	6.74	0.18		6136.1	7.21	0.06
	4937.2	7.48	0.03		6170.1	6.07	0.86
	5001.5	7.10	0.08		6200.3	6.81	0.16
	5039.7	7.09	0.08		6238.9	7.55	0.03
	5118.8	6.81	0.15		6251.9	6.88	0.13
$(5/2)$	5124.6	6.30	0.50		6264.3	7.01	0.11
$(9/2^-)$	5149.4	5.66	2.18		6286.3	7.37	0.04
$(9/2)$	5167.4	6.89	0.13		6314.8	5.64	2.32
	5191.1	7.38	0.04		6326.6	6.79	0.16
	5276.6	6.35	0.45		6348.8	5.97	1.07
	5302.6	6.98	0.10		6364.2	6.43	0.37
	5325.6	7.61	0.03		6411.5	6.39	0.41
	5376.0	6.22	0.61		6445.1	6.28	0.53
	5402.5	7.54	0.03		6457.7	6.05	0.90
	5413.2	7.12	0.08		6497.9	6.37	0.42
	5421.4	7.63	0.02		6505.4	6.24	0.58
	5427.8	7.94	0.01		6514.9	6.43	0.37
	5450.9	7.94	0.01		6576.2	6.71	0.20
	5483.1	6.08	0.84		6705.7	6.74	0.18
	5485.0	6.61	0.25	$(9/2)$	6770.6	6.43	0.37
	5493.5	7.13	0.08		6794.4	6.63	0.24
	5548.3	7.49	0.03		6950.7	6.00	0.99
	5559.9	5.73	1.84				

<sup>a</sup>Deduced using the tables of Gove and Martin [37] and a half-life of 1.32 s [8].<sup>b</sup> $\log f_1 t = 9.3$  and  $1/f_1 t = 0.0005 \times 10^{-6}$ .

level of  $^{133}\text{Sb}$ , but no significant population of the higher lying single-proton states.

In Table II we present the experimental single-proton energies in  $^{133}\text{Sb}$  compared to the values predicted in the theoretical works of Refs. [17–19] and from realistic shell model (RSM) calculations. The theoretical single particle energies displayed in column labeled WS+ $\Delta$ , were obtained in Ref. [17] from a Woods-Saxon calculation using  $^{208}\text{Pb}$  parameters except for the central well depths for neutrons and protons, which were adjusted “ad hoc” to the data in the  $^{132}\text{Sn}$  region. The energies listed in columns 3–5 were calculated [18] using three different models. The first two models make use of single particle Woods-Saxon (WS) and folded Yukawa (FY) potentials, respectively, while the Hartree-Fock method with the Skyrme III interaction (SIII) is applied in the third model. Column seven, labeled SKX, shows the values recently obtained [19] from a fit of six out of the ten conventional Skyrme-interaction parameters to a large body of data related to the nuclear ground state properties. Note, that in the fitting of these parameters an incorrect value of 2.71 MeV for the single particle energy for the  $d_{3/2}$  state has been used [19]. In spite of this, the new excitation energy for the  $3/2^+$  state, see Table II, is in better agreement with the SKX prediction for the  $d_{3/2}$ . However, the  $5/2^+$  state differs from the calculated  $d_{5/2}$  value by 400 keV, but that is within the rms deviation of 490 keV found for the other states around  $^{132}\text{Sn}$ .

The last column (RSM) of Table II lists the values derived from a realistic shell-model calculation, which is discussed here in some detail. By taking the doubly magic  $^{100}\text{Sn}$  as a closed core, a two-body realistic effective interaction  $V_{\text{eff}}$  has been derived from the meson-theoretic Bonn A nucleon-nucleon potential [20] in the model space consisting of the five single-particle orbitals  $0g_{7/2}$ ,  $1d_{5/2}$ ,  $2s_{1/2}$ ,  $1d_{3/2}$ , and  $0h_{11/2}$ . This derivation was carried out within the framework of a  $G$ -matrix folded-diagram formalism, including renormalizations from both core polarization and folded diagrams. Calculations with this effective interaction were performed on the light Sn isotopes [21,22] and the particle-hole  $^{132}\text{Sb}$  nucleus [23]. Obviously, in the former case only  $T=1$  matrix elements are needed.

The single-particle energies at the  $^{100}\text{Sn}$  region are not known experimentally. In Ref. [21] the single-neutron energies were determined from an analysis of the low-energy spectra of the Sn isotopes having  $A \leq 111$ . For  $^{133}\text{Sb}$ , the single-particle energies are assumed to be equal for protons and neutrons with the adopted values  $\epsilon_{d_{5/2}}=0$ ,  $\epsilon_{g_{7/2}}=0.20$ ,  $\epsilon_{s_{1/2}}=1.72$ ,  $\epsilon_{d_{3/2}}=1.88$ , and  $\epsilon_{h_{11/2}}=2.70$  MeV, which are just the same as those used in the calculation on  $^{132}\text{Sb}$  [23]. As compared to the single-neutron energies used for the Sn isotopes, only  $\epsilon_{s_{1/2}}$  and  $\epsilon_{d_{3/2}}$  have different values, both being decreased by about 0.5 MeV. In fact, the position of these two levels is very important to satisfactorily reproduce the experimental  $1_2^+$  state and place the calculated negative-parity states in the right energy range in  $^{132}\text{Sb}$  (see Ref. [23]), while it plays a minor role in the calculations on the light Sn isotopes.

The theoretical energies of the single-proton states in  $^{133}\text{Sb}$  are obtained by the following relation:

$$E_j(^{133}\text{Sb}) = \epsilon_j + \Delta_j, \quad (1)$$

where  $\epsilon_j$  are the single particle energies given above, and

$$\Delta_j = \frac{1}{2(2j+1)} \sum_{j_n j_T} (2J+1) G_{JT}(j_n j j_n j). \quad (2)$$

The  $G$ 's are the two-body matrix elements of the effective interaction  $V_{\text{eff}}$  between states that are antisymmetrized but not normalized. Table II illustrates the calculated spectrum of  $^{133}\text{Sb}$ . It appears that the energies of the  $5/2^+$ ,  $3/2^+$ , and  $11/2^-$  states are quite well reproduced by the theory, the largest discrepancy being about 180 keV for the  $5/2^+$  state.

Our new experimental results on the single-particle states in  $^{133}\text{Sb}$  give the first possibility to compare the  $d_{5/2}-d_{3/2}$  spin orbit splitting with theoretical predictions. The calculations in Refs. [17,19] and the RSM give values near the experimental results. Table II illustrates also that the binding of the  $d_{5/2}$  state relative to the ground state, vary strongly between different calculations. This is also the case for the still missing  $s_{1/2}$  state. The quality of the comparison between the theoretical and experimental single particle energies for  $^{132}\text{Sn}$  is comparable to that of  $^{208}\text{Pb}$  in the SKX fit of Ref. [19]. Based upon the systematic underbinding found for the calculated s and p particle states in  $^{208}\text{Pb}$ , one would expect that the  $s_{1/2}$  level in  $^{133}\text{Sb}$  may appear experimentally at an excitation energy which is up to 1.0 MeV lower than given by SKX. In this case the “best” calculations of Refs. [17,19] and RSM would predict the  $1/2^+$  state to appear at about 2 MeV.

We finally note, that the single proton energies measured in the present experiment are used in Ref. [24] to construct a new theoretical single particle spectrum at  $^{132}\text{Sn}$  using a new parameter set of the Nilsson potential. The new Nilsson parameters allow to construct a better basis of wave functions in order to study ground state and collective excitations in the region near  $^{132}\text{Sn}$ . This has been demonstrated in the case of the yrast band in  $^{136}\text{Te}$  studied using the projected shell model (PSM) [24].

For completeness we also present here the experimental results on single proton transition rates already discussed in Ref. [10]. The  $\gamma$ -ray branching from the  $d_{3/2}$  level allows to determine the following ratio:  $B(M1; d_{3/2} \rightarrow d_{5/2})/B(E2; d_{3/2} \rightarrow g_{7/2}) = 0.037(3)$  when the transition rates are expressed in Weisskopf units (W.u.), which is found to be remarkably similar to the value  $B(M1; f_{5/2} \rightarrow f_{7/2})/B(E2; f_{5/2} \rightarrow h_{9/2}) = 0.031(3)$  obtained for the single-proton nucleus  $^{209}\text{Bi}$ .

For the  $h_{11/2}$  state at 2791.3 keV, a half-life of 11.4(4.5) ps and the  $\gamma$ -ray branching to the  $d_{5/2}$  state were measured for the first time. From these data we obtain a value of  $B(M2; h_{11/2} \rightarrow g_{7/2}) = 0.55(22)$  W.u. that represents a very high  $M2$  transition rate. The  $\gamma$ -ray branching of the  $E3$  transition gives  $B(E3; h_{11/2} \rightarrow d_{5/2}) = 22(13)$  W.u., which is comparable to the recently [2] deduced  $B(E3)$  of about 15 W.u. for the core. See Ref. [10] for a further discussion of

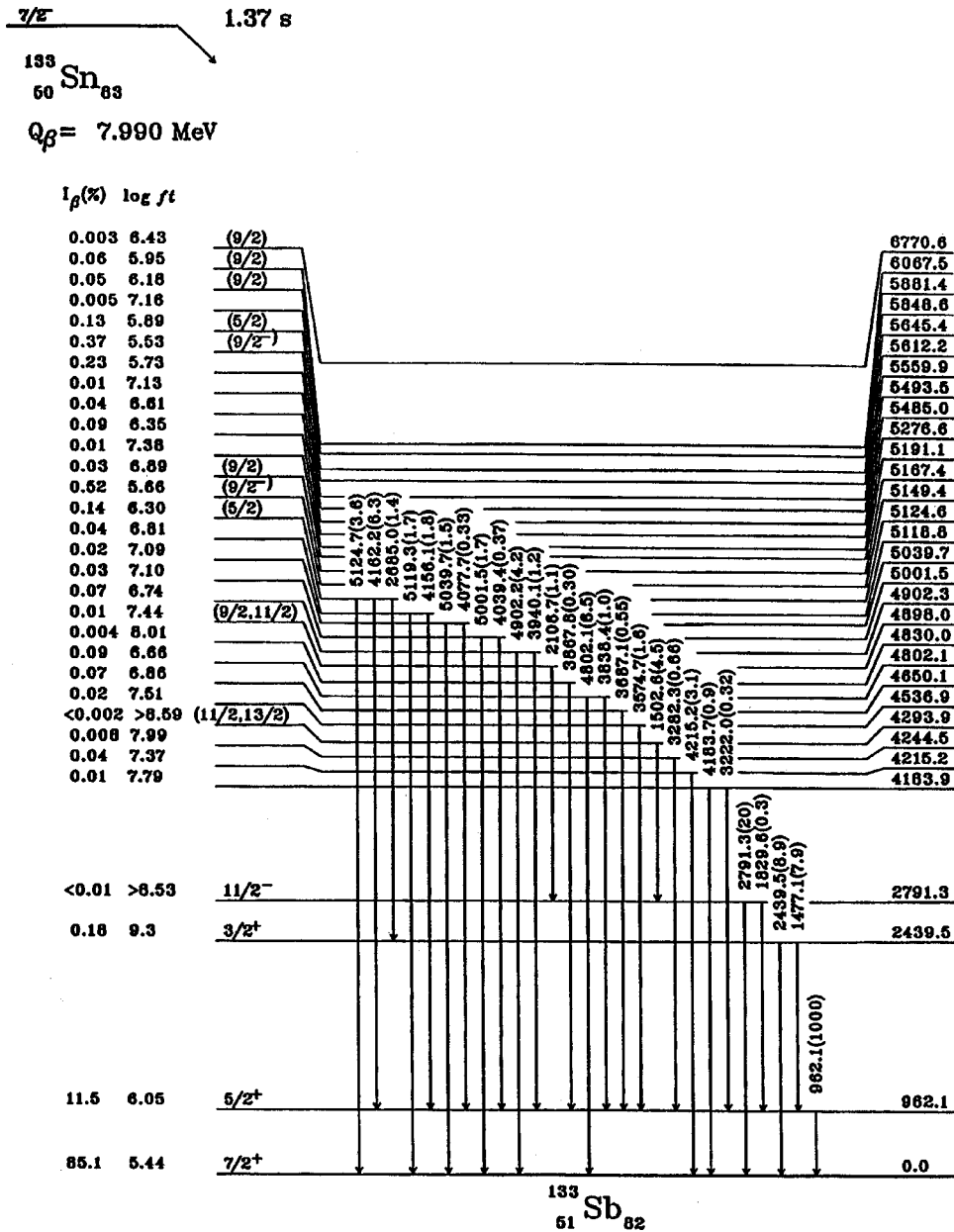


FIG. 2. Partial level scheme of  $^{133}\text{Sb}$  containing levels with a significant  $\gamma$ -ray branching to lower lying states. Tentative values of spin and parity assignments are based on the observed branchings to either the  $d_{3/2}$  or  $h_{11/2}$  single-proton states. See text for details.

these single proton transition strengths in  $^{133}\text{Sb}$  and a comparison with the corresponding transitions in the single-proton nucleus  $^{209}\text{Bi}$ .

**B. Core-coupled states**

Apart from the single-proton states discussed above, the present experiment revealed about ninety additional levels in the excitation energy from 4 to 7 MeV. The  $\beta$ -decay energy window extends up to 8 MeV, but the rapidly decreasing intensity with the decreasing  $\beta$ -transition energy will in practice prohibit a detectable population of the states above 7 MeV.

The main information regarding the high lying states of  $^{133}\text{Sb}$  is found in Tables I and III. The partial level scheme

shown in Figs. 2 and 3 contains only those levels which had a significant  $\gamma$ -ray branching to lower lying states. The present data alone do not permit firm conclusions regarding spins and parities of the high lying states. The tentative values shown are based on the observed branchings to either the  $d_{3/2}$  or  $h_{11/2}$  single-proton states. Some high-lying levels are populated with  $\beta$ -transitions of a sufficient strength to be of Gamow-Teller type. A negative parity is thus tentatively assigned in these cases.

The low-lying single-proton states in  $^{133}\text{Sb}$  can couple to the excitations in  $^{132}\text{Sn}$  giving rise to a number of different multiplets of core-coupled states at energies of about 4 MeV and higher. In a first order approximation, more than 150 possible configurations with spins ranging from  $1/2^+$  to  $21/2^+$  for the positive parity levels, and from  $1/2^-$  to  $23/2^-$

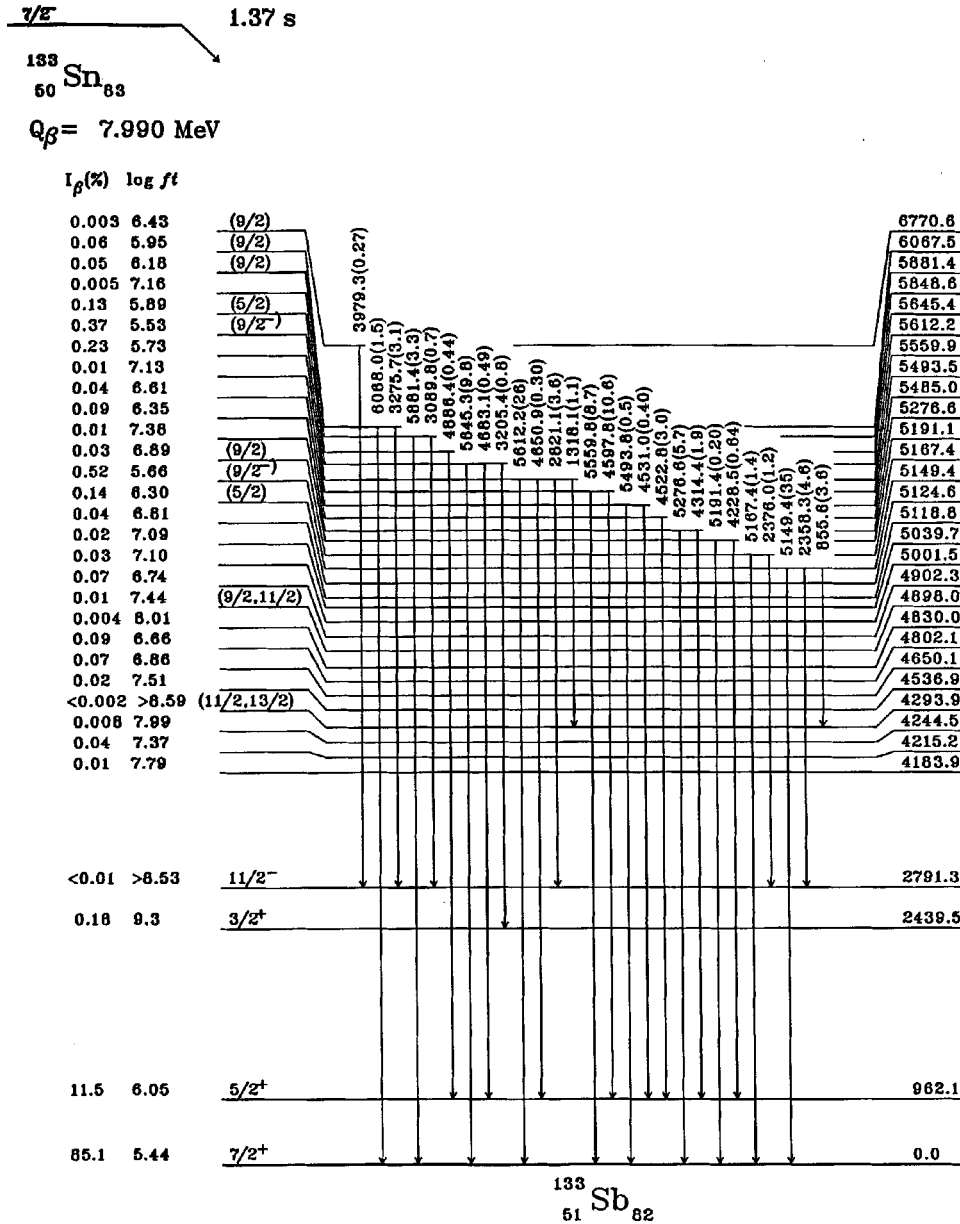


FIG. 3. Partial level scheme of  $^{133}\text{Sb}$  (continuation).

for the negative parity states, are expected to exist at the excitation energy from 4 to 7 MeV. However only some of these levels will be directly populated in the  $\beta^-$ -decay of  $^{133}\text{Sn}$ , since only allowed and first-forbidden  $\beta$ -transitions could be expected to give a detectable population of states in  $^{133}\text{Sb}$ . The ground state of  $^{133}\text{Sn}$  has  $J^{\pi} = 7/2^-$ , therefore the levels directly populated in the  $\beta$ -decay would have  $J^{\pi}$  extending from  $5/2^-$  to  $9/2^-$  and from  $3/2^+$  to  $11/2^+$ .

There are only three known (and expected) core states in  $^{132}\text{Sn}$  at excitation energy of 4.4 MeV or below, having  $J^{\pi} = 2^+, 3^-,$  and  $4^+$ . We observe 11 levels in  $^{133}\text{Sb}$  at 4.0–4.4 MeV, of which one is significantly populated only by  $\gamma$ -rays from higher lying states. It is quite likely that these particular levels, belong to the three multiplets expected from a coupling of the  $g_{7/2}$  proton to the lowest core states. We can with some certainty assign the two lowest collective

levels in  $^{133}\text{Sb}$ , at 4028.7 and 4060.2 keV, as members of the core  $2^+$  multiplet. In general the  $\beta$ -decay data alone are not sufficient for an experimental identification of multiplet members. One may compare with the situation in  $^{209}\text{Bi}$  where the lowest core multiplet, formed by the collective  $3^-$  at 2.61 MeV coupled to the  $h_{9/2}$  proton, is well known experimentally [25]. However, the experimental splitting of the multiplet levels could not be reproduced by the detailed theoretical analysis of Hamamoto [26,27], since the theoretical uncertainties in, e.g., interaction energies turns out to be comparable to the total splitting of the multiplet.

The rapidly increasing density of expected core-coupled states in  $^{133}\text{Sb}$  at energies above 4.5 MeV is reflected in the large number of levels observed in our experiment, and prohibits a meaningful identification of individual members of a given multiplet, except in special cases. One such special

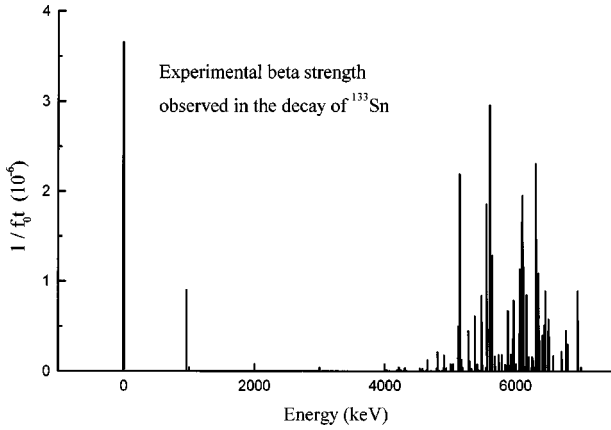


FIG. 4.  $\beta$ -strength observed in the decay of  $^{133}\text{Sn}$  versus excitation energy in  $^{133}\text{Sb}$ .

case is offered by the extremes of angular momenta. It appears thus quite likely that the 16  $\mu\text{s}$  isomer previously observed by Sistemich *et al.* [8] can be identified with one of the states of high angular momentum in the core( $8^+$ )  $\otimes$   $g_{7/2}$  multiplet. The level observed by us at 4293.9 keV, decaying strongly to the  $h_{11/2}$  state, is likely to belong to one of the core( $3^-$ )  $\otimes$   $g_{7/2}$  or core( $4^+$ )  $\otimes$   $g_{7/2}$  multiplets.

### C. The $\beta$ -decay properties of $^{133}\text{Sn}$

The  $\beta$ -transitions between valence nuclei at the doubly closed shells offer some of the best opportunities for detailed comparisons between experiments and the theory of nuclear  $\beta$ -decay. The wave functions of the odd nucleon states are known rather accurately, allowing precise calculations of the matrix elements for the  $\beta$ -transitions between the single particle states. The present experiments have resulted in new data for the first forbidden unique transition to the  $d_{3/2}$  state and much improved information on the decays to the higher lying states above 4 MeV in the daughter nucleus. The latter states are sufficiently widely spaced to permit discrete level spectroscopy. An analysis in terms of a  $\beta$ -strength function [28] may be appropriate. The tabulated experimental data on the observed  $\beta$ -transitions, see Table III, therefore include values of both  $\log f_0 t$  and the inverse  $1/f_0 t$ . The latter is proportional to the  $\beta$ -strength shown in Fig. 4. Our  $\gamma$ -ray measurements did not reveal any  $^{133}\text{Sb}$  levels above about 7 MeV due to the decreasing absolute  $\beta$  intensities, a somewhat reduced  $\gamma$ -ray detection efficiency, and the opening of the neutron emission channel at about 7.1 MeV. The delayed neutron emission in the decay of  $^{133}\text{Sn}$  is 0.0294(24)% [29]. The  $\beta$  feeding of the unbound levels is thereby compatible with the average  $\beta$ -strength observed at 4–7 MeV. A  $Q_{\beta}$ -decay energy of 7990 keV [30] was used to derive the values given in the table. Below, we discuss first the transitions to the single-proton states followed by some comments on the  $\beta$  feeding of the higher excited states.

The first strong peak shown in Fig. 4 represents the decay of the  $f_{7/2}$  neutron in  $^{133}\text{Sn}$  to the  $g_{7/2}$  ground state of  $^{133}\text{Sb}$ . This transition is a spin flip  $\Delta J=0$  first-forbidden one with a  $\log(f_0 t)_{\text{exp}}=5.44$ . The analogous transition  $\nu g_{9/2} \rightarrow \pi h_{9/2}$  in the decay of  $^{209}\text{Pb}$  has a similar value [25] of  $\log(f_0 t)_{\text{exp}}$

TABLE IV. Comparison of experimental and predicted shape factors  $\langle C(W) \rangle^{1/2}$  for the first-forbidden single particle  $\beta^-$  transitions of the decay of  $^{133}\text{Sn}$ . H7B and HBB denote theoretical values obtained using different residual interactions; see [33,35] for an explanation of the notation.

Transition	$E_{\text{level}}$ (keV)	$\log f_0 t$	$\langle C(W) \rangle^{1/2}$		
			Expt.	H7B	HBB
$\nu f_{7/2} \rightarrow \pi d_{5/2}$	962.1	6.05	28.8	37.3	40.0
$\nu f_{7/2} \rightarrow \pi d_{3/2}$	2439.5	7.42	5.9	2.4	3.4

$=5.534$ . The latter transition has been subject to extensive theoretical studies [31–33]. The existence of very fast, first-forbidden transitions in the region of  $^{208}\text{Pb}$  is well known and, on the whole, can be reproduced by the shell model calculations [34]. In particular, it was shown by Damgaard and Winther [31] that this decay proceeds essentially through matrix elements of multipolarity 0; i.e., the decay is dominated by the pseudoscalar  $\vec{\sigma} \cdot \vec{r}$  operator. A strong similarity is expected for the transition in the  $^{133}\text{Sn}$  decay. The detailed analysis by Chou and Warburton [35] shows that the rank-1 and rank-2 contributions to this branch are of the order of 1.4%, implying that the branch to the  $g_{7/2}$  ground state is nearly purely of multipolarity 0.

The second peak in Fig. 4 represents the first-forbidden  $\beta$ -transition to the single-proton  $d_{5/2}$  level. A comparison of experiment and theory [35] for the  $\Delta J \neq 0$  first-forbidden decays to the  $d_{3/2}$  and  $d_{5/2}$  single-proton states in  $^{133}\text{Sb}$  is made in Table IV. This comparison is formulated via the square root of the averaged shape factor,  $\langle C(W) \rangle^{1/2}$  (corresponding to the experimental value of the rank-0 matrix element), as defined in Ref. [33]. The experimental shape factors of Table IV are derived according to Ref. [33] as

$$\langle C(W) \rangle = 9195 \times 10^5 / f_0 t \text{ fm}^2. \quad (3)$$

The shape factor modifies the allowed shape of the  $\beta$  spectrum extending from  $W=1$  to  $W_0$ , where  $W_0$  is the total disintegration energy. The  $\nu f_{7/2} \rightarrow \pi d_{5/2}$  transition to the level at 962.1 keV [ $\log(f_0 t)_{\text{exp}}=6.05$ ] does not flip the spin. This  $\Delta J=1$  decay is dominated by rank-1 operators with some cancellation between  $\vec{r}$  and  $\vec{\sigma} \times \vec{r}$  operators. The rank-2 contribution is estimated [35] to be less than 10%. The calculated shape factors agree with experiment within the experimental uncertainty.

The  $\Delta J=2$  decay to the state at 2439.5 keV,  $\nu f_{7/2} \rightarrow \pi d_{3/2}$  represents a first-forbidden unique transition with spin flip and is therefore much too slow to be visible on the scale of Fig. 4; in this case the  $\log(f_0 t)_{\text{exp}}=7.42$ , while the  $\log(f_1 t)_{\text{exp}}=9.30$ . The transition is sufficiently slow that admixtures to the wave function are of importance to the strength. The analysis by Chou and Warburton [35] shows that admixtures from several p-h transitions may occur but only the one involving the  $\nu h_{11/2} \rightarrow \pi g_{7/2}$  transition is of importance, through a  $\{\nu f_{7/2} \otimes [\pi g_{7/2} \nu h_{11/2}^{-1}]_{3/2^+}\}$  admixture in the final state. A major reason for the importance of the admixture of this p-h state is the relatively high excitation energy of the  $d_{3/2}$  level, bringing it closer to the core-coupled states. The authors of Ref. [35] conclude that their calcula-

tion is somewhat uncertain due to the noninclusion of admixtures which contain configurations outside the model space. Inspection of Table IV shows, however, that the calculated shape correction factor is within a factor of two from the experimental one. The  $\Delta J=2$  transition to the 2791.3 keV single-proton level,  $\nu f_{7/2} \rightarrow \pi h_{11/2}$ , is of the second forbidden nonunique type, and too slow to be observed experimentally.

We now turn our attention to the core excited states. We give here only some general remarks on  $\beta$ -transitions that contribute to the  $\beta$ -strength in the region above 4 MeV of excitation energy. We noted above that the first-forbidden transition to the  $\pi g_{7/2}$  ground state of  $^{133}\text{Sb}$  is unusually fast. In contrast, the transition feeding the  $\pi g_{9/2}^{-1}$  spin orbit partner, present at about 5.5 MeV, is expected to be relatively slow. This is mainly because the high occupancy of the  $\pi g_{9/2}$  orbital below the Fermi surface blocks the transition. A  $\log f_0 t \geq 7$  is thus suggested for the  $\nu f_{7/2} \rightarrow \pi g_{9/2}^{-1}$  transition. The absence of a strong  $\beta$  feeding to the proton hole state prohibits an identification of this state using the present data.

The dominant decay involving the core neutrons is expected to proceed by Gamow-Teller transitions. In the decay

of the core  $^{132}\text{Sn}$  itself [36] about 99% of the intensity feeds a  $1^+$  state in  $^{132}\text{Sb}$  at 1325 keV with the main configuration  $\pi d_{5/2} \nu d_{3/2}^{-1}$ . The  $\beta$ -transition energy should be about the same for  $^{133}\text{Sn}$  as for  $^{132}\text{Sn}$ :  $3108-1325 = 1783$  keV, leading to a group of  $5/2^-$ ,  $7/2^-$ ,  $9/2^-$  levels in  $^{133}\text{Sb}$  near  $7990-1783=6207$  keV. The transitions are fragmented over many final states in a wide (MeV) region of energy. The total observed strength to levels above 5 MeV in  $^{133}\text{Sb}$  (see Table III) is  $\Sigma 1/f_0 t = 33 \times 10^{-6}$ , i.e., about one third of the strength to the dominant  $1^+$  state in  $^{132}\text{Sb}$  with  $\log f_0 t = 4.01$ . A major part of the missing strength is likely to occur in many levels in the 6–8 MeV region, where the increasing level density, the decreasing phase space, and the opening of the neutron emission channel all tend to make the detection of discrete gamma rays difficult.

### ACKNOWLEDGMENTS

Comments by B.A. Brown are gratefully acknowledged. The authors wish to thank L. Jacobsson and P. Jonsson for their expert operation of OSIRIS. The work was supported by the Swedish Natural Science Research Council.

- 
- [1] P. Hoff *et al.*, Phys. Rev. Lett. **77**, 1020 (1996).  
 [2] J. P. Omtvedt, H. Mach, B. Fogelberg, D. Jerrestam, M. Hellström, L. Spanier, K. I. Erokhina, and V. I. Isakov, Phys. Rev. Lett. **75**, 3090 (1995).  
 [3] N. J. Stone, D. Doran, M. Lindroos, J. Rikovska, M. Veskovica, G. White, D. A. Williams, B. Fogelberg, L. Jacobsson, I. S. Towner, and K. Heyde, Phys. Rev. Lett. **78**, 820 (1997).  
 [4] C. T. Zhang *et al.*, Phys. Rev. Lett. **77**, 3743 (1996).  
 [5] C. T. Zhang *et al.*, Z. Phys. A **358**, 9 (1997).  
 [6] P. Bhattacharyya *et al.*, Phys. Rev. C **56**, R2363 (1997).  
 [7] S. Borg, G. B. Holm, and B. Rydberg, Nucl. Phys. **A212**, 197 (1973).  
 [8] K. Sistemich, W.-D. Lauppe, T. A. Khan, H. Lawin, H. A. Selic, J. P. Bocquet, E. Monnard, and F. Schussler, Z. Phys. A **285**, 305 (1978).  
 [9] J. Blomqvist, A. Kerek, and B. Fogelberg, Z. Phys. A **314**, 199 (1983).  
 [10] M. Sanchez-Vega, B. Fogelberg, H. Mach, R. B. E. Taylor, A. Lindroth, and J. Blomqvist, Phys. Rev. Lett. **80**, 5504 (1998).  
 [11] B. Fogelberg *et al.*, Nucl. Instrum. Methods Phys. Res. **B 70**, 137 (1992).  
 [12] S. Rab, Nucl. Data Sheets **75**, 491 (1995).  
 [13] M. L. Stelts and R. E. Chrien, Nucl. Instrum. Methods **155**, 253 (1978).  
 [14] E. B. Shera, Phys. Rev. C **12**, 1003 (1975).  
 [15] H. Mach, R. L. Gill, and M. Moszyński, Nucl. Instrum. Methods Phys. Res. A **280**, 49 (1989), and references therein.  
 [16] G. Audi and A. H. Wapstra, Nucl. Phys. **A565**, 66 (1993).  
 [17] J. Blomqvist, in *Proceedings of the 4th International Conference on Nuclei Far From Stability*, Helsingor, 1981 (CERN, Geneva, 1981), p. 536.  
 [18] G. A. Leander, J. Dudek, W. Nazarewicz, J. R. Nix, and Ph. Quentin, Phys. Rev. C **30**, 1 (1984).  
 [19] B. A. Brown, Phys. Rev. C **58**, 220 (1998).  
 [20] R. Machleidt, K. Holinde, and Ch. Elster, Phys. Rep. **149**, 1 (1987).  
 [21] F. Andreozzi, L. Coraggio, A. Covello, A. Gargano, T. T. S. Kuo, Z. B. Li, and A. Porrino, Phys. Rev. C **54**, 1636 (1996).  
 [22] A. Covello, F. Andreozzi, L. Coraggio, A. Gargano, T. T. S. Kuo, and A. Porrino, Prog. Part. Nucl. Phys. **38**, 165 (1997).  
 [23] F. Andreozzi, L. Coraggio, A. Covello, A. Gargano, T. T. S. Kuo, and A. Porrino, Phys. Rev. C **59**, 746 (1999).  
 [24] J. Zhang, Y. Sun, M. Guidry, L. L. Riedinger, and G. A. Lalazissis, Phys. Rev. C **58**, R2663 (1998).  
 [25] M. J. Martin and J. K. Tuli, Nucl. Data Sheets **63**, 723 (1991).  
 [26] I. Hamamoto, Nucl. Phys. **A126**, 545 (1969).  
 [27] I. Hamamoto, Nucl. Phys. **A135**, 576 (1969).  
 [28] C. L. Duke, P. G. Hansen, O. B. Nielsen, and G. Rudstam, Nucl. Phys. **A151**, 609 (1970).  
 [29] G. Rudstam, K. Aleklett, and L. Sihver, At. Data Nucl. Data Tables **53**, 1 (1993).  
 [30] K. A. Mezilev *et al.*, Phys. Scr. **T56**, 272 (1995).  
 [31] J. Damgaard and A. Winther, Nucl. Phys. **54**, 615 (1964).  
 [32] H. Behrens, M. Kobelt, W. G. Thies, and H. Appel, Z. Phys. **252**, 349 (1972).  
 [33] E. K. Warburton, Phys. Rev. C **44**, 233 (1991).  
 [34] J. Damgaard, R. Broglia, and C. Riedel, Nucl. Phys. **A134**, 310 (1969).  
 [35] W. T. Chou and E. K. Warburton, Phys. Rev. C **45**, 1720 (1992).  
 [36] C. A. Stone, S. H. Faller, and W. B. Walters, Phys. Rev. C **39**, 1963 (1989).  
 [37] N. B. Gove and M. J. Martin, Nucl. Data Tables **10**, 205 (1971).